THE JOURNAL OF PHYSICAL CHEMISTRY B

Article

pubs.acs.org/JPCB

Complexity of the Folding Transition of the B Domain of Protein A Revealed by the High-Speed Tracking of Single-Molecule Fluorescence Time Series

Hiroyuki Oikawa,[†] Kiyoto Kamagata,[†] Munehito Arai,[‡,§] and Satoshi Takahashi*[,†]

[†]Institute of Multidisciplinary Research for Advanced Materials, Tohoku University, 2-1-1 Katahira, Aoba, Sendai, Miyagi 980-8577, Japan

[‡]Department of Life Sciences, Graduate School of Arts and Sciences, The University of Tokyo, 3-8-1 Komaba, Meguro, Tokyo 153-8902, Japan

[§]PRESTO, Japan Science and Technology Agency, 4-1-8 Honcho, Kawaguchi, Saitama 332-0012, Japan

Supporting Information

ABSTRACT: The equilibrium unfolding transition of the B domain of protein A (BdpA) was investigated by using single-molecule fluorescence spectroscopy based on line-confocal detection of fast-flowing samples. The method achieved the time resolution of 120 μs and the observation time of a few milliseconds in the single-molecule time-series measurements of fluorescence resonance energy transfer (FRET). Two samples of BdpA doubly labeled with donor and acceptor fluorophores, the first possessing fluorophores at residues 22 and 55 (sample 1) and the second at residues 5 and 55 (sample 2), were prepared. The equilibrium unfolding transition induced by guanidium chloride (GdmCl) was monitored by bulk measurements and demonstrated that the both samples obey the apparent two-state unfolding. In the absence of GdmCl, the single-molecule FRET measurements for the both samples showed a single peak assignable to the native state (N). The FRET efficiency for N shifts to lower values as the increase of GdmCl concentration, suggesting the swelling of the native state structure. At the higher concentration of GdmCl, the both samples convert to the unfolded state (U). Near the unfolding midpoint for sample 1, the kinetic exchange between N and U causes the averaging of the two states and the higher values of the relative fluctuation. The time series for different molecules in U showed slightly different FRET efficiencies, suggesting the apparent heterogeneity. Thus, the high-speed tracking of fluorescence signals from single molecules revealed a complexity and heterogeneity hidden in the apparent two-state behavior of protein folding.

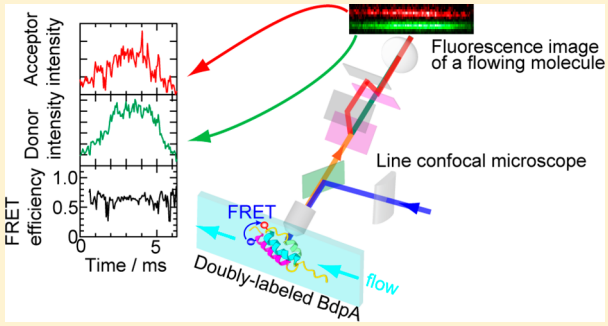

INTRODUCTION

Proteins are natural heteropolymers that can fold autonomously from the unfolded state having properties of random coil to the native state with specific three-dimensional structures.[1−7] The folding and unfolding of small proteins with roughly fewer than 100 residues usually occurs as a cooperative two-state transition between the unfolded state and the native state.[8−10] Several small proteins called downhill folding proteins do not obey the two-state mechanism and change the average conformations continuously with only one state in one condition.[11] In addition, the two-state transition might not be perfect or can be converted to the three-state transition easily.[12,13] However, simple and cooperative folding transitions are generally observed for many small proteins.

Single-molecule fluorescence spectroscopy (SMFS) is a powerful method for the investigation of protein conformations and dynamics.[14−17] The method is based on the labeling of two fluorophores acting as donor and acceptor to specific residues of a protein. Upon the excitation of the donor and the detection of fluorescence intensities of the both fluorophores at the single-molecule level, the distance between them can be deduced from the efficiency of the fluorescence resonance energy transfer (FRET). The method can detect inhomogeneous distributions of protein structures and is expected to resolve substates in the unfolded ensemble and the connectivity of the substates that are essential to understand the reaction coordinate and the foldability of proteins.[18−21] Accordingly, SMFS has been extensively applied for the elucidation of folding transition of proteins.[22−27]

Despite the advantages of SMFS, however, the method based on conventional detection system suffers from a limited time resolution in determining of the FRET efficiency. In typical experiments, a cell containing a solution of the doubly labeled sample is placed at the focal point of the confocal fluorescence

Received: January 15, 2015
Revised: April 6, 2015
Published: May 4, 2015

DOI: 10.1021/acs.jpcb.5b00414
J. Phys. Chem. B 2015, 119, 6081−6091

microscope.[14−17] The diffusing samples give bursts of fluorescence that last several milliseconds and consist of several tens of photons. Because of the saturation at intense excitation, it is difficult to obtain larger numbers of photons from a single burst. Since the number of photons required to estimate the FRET efficiency with reasonable accuracy is several tens, the time resolution of the conventional single-molecule FRET (sm-FRET) measurements is limited to several milliseconds. Muñoz and his collaborators achieved the time resolution of 50 μs using additives that can suppress the saturation of fluorescence intensity at intense excitations.[28] However, the past investigations using SMFS are mostly based on the information in the time domain longer than several milliseconds.

In our previous investigation, we developed a new method of SMFS, a line confocal microscopy, and improved the time resolution of sm-FRET efficiency measurements to several tens of microseconds.[29] The method is based on the finding of Horrocks et al. that the number of fluorescence photons from single molecules can be increased significantly if a fast sample flow is coupled to confocal microscopy.[30] We confirmed the observation and could increase the number of photon detection to several thousands per millisecond without using any additives. We proposed that the lowest excited triplet state of fluorophore, which is formed occasionally during the intense excitation and causes the saturation, is quenched by fresh oxygen molecules continuously supplied by the flow system. While the residence time of molecules in the focal point of the conventional confocal microscopy becomes extremely short under the fast flow, we introduced the line confocal system, in which a line-shaped excitation light is focused along the microfluidic channel and can excite flowing molecules continuously. We could obtain time series of sm-FRET efficiency for the duration of several milliseconds with time resolution of 120 μs. Using the B domain of protein A (BdpA) as the first model, we demonstrated the feasibility of the method.

BdpA is one of the most intensively studied proteins for the elucidation of protein folding mechanism. The protein is composed of 60 residues and possesses three helices: helix 1 (residues 10−19), helix 2 (residues 25−37), and helix 3 (residues 42−56), which were separated by turn 1 (residues 20−24) and turn 2 (residues 38−41) (Figure 1).[31] The N-terminal region up to the middle of helix 1 and the C-terminal half of helix 3 are fluctuating.[31,32] The folding of BdpA obeys the two-state mechanism, whose folding rate constant in the absence of denaturant exceeds 10^5 s^{-1}.[32−34] Among the three helices, helix 3 possesses the highest helix propensity, as demonstrated for synthetic polypeptides corresponding to each helix.[32] However, the Φ-value analysis demonstrated that helix 2 is mainly formed in the folding transition state.[35−37] The sm-FRET measurements in the millisecond time domain demonstrated the two-state transition of BdpA.[38,39] The fluorescence lifetime measurements suggested the presence of a compact structure in the unfolded state near the midpoint of folding transition.[40]

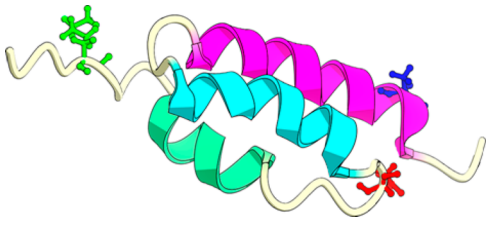

Figure 1. Native structure of the wild-type BdpA determined by solution NMR (PDB ID: 1BDD).[31] The helices 1, 2, and 3 are colored light green, light blue, and pink, respectively. In sample 1, residues 22 (red) and 55 (blue) were labeled. In sample 2, residues 5 (green) and 55 (blue) were labeled.

The small size and the fast folding of BdpA make the protein one of ideal targets for the theoretical investigations.[41−45] The early investigations suggested the initial formation of helix 3 followed by the formation and packing of other helices,[42,43,45] which do not agree with the results of the Φ-value analysis.[35−37] It was proposed that BdpA may take different folding pathway by small changes of temperature.[46] However, the subsequent Φ-value analysis showed that the order of helix formation does not depend on temperature.[37] A recent molecular dynamics calculation suggested that the folding mechanism of BdpA converts from the two-state folding to the downhill folding upon the increase in temperature.[47] The misfolded conformations possessing a mirror-image arrangement of the helices was also proposed.[47,48]

In our previous report, various properties of BdpA were revealed through the examination of the sm-FRET traces.[29] We introduced the donor and acceptor fluorophores at turn 1 and C-terminus and detected distributions assignable to the native and unfolded states, suggesting the two-state folding transition. Furthermore, we characterized the dynamic property of the observed traces by introducing a quantity, relative fluctuation (RF), which is the variance of each trace divided by the shot noise width estimated from the average photon number of the trace. We observed that the traces obtained near the unfolding transition possess larger values of RF, suggesting the dynamic changes of the observed traces. However, the sample showed significant fluorescence quenching in the native state likely due to the proximity of the labeling sites.

In this investigation, we constructed a new mutant of BdpA introducing fluorophores near the N and C termini to avoid the quenching effect. We observed sm-FRET time series of the new sample by the line confocal system at different concentrations of denaturant and compared the obtained traces to those of the previous sample. Furthermore, we improved the data analysis procedures and calibrated the FRET efficiencies using the fluorescence quantum yields and the detector efficiencies. We also improved the method of estimating the RF values by incorporating the noise contribution from the background. Our observation revealed significant complexity in the apparent two-state transition of BdpA.

EXPERIMENTAL SECTION

Expression, Purification, and Labeling of BdpA and the Bulk Characterization of the Labeled Samples. The expression and purification of the triple mutants of BdpA were performed as reported previously.[29] In brief, a gene fragment of the triple mutant for sample 1 with an N-terminal His tag and a thrombin-cleaving site was synthesized and ligated into a plasmid (pUC19, Takara Bio Inc., Shiga, Japan). The mutations for sample 2 were introduced according to the method described in the QuikChange site-directed mutagenesis kit (Agilent Technologies, Santa Clara, CA) with modifications. The *E. coli* JM109 cells containing the plasmid vector were grown overnight and harvested. The supernatant of the lysed cells was applied to a nickel chelating column (NiNTA Superflow, Qiagen) and washed. The column was incubated

DOI: 10.1021/acs.jpcb.5b00414
J. Phys. Chem. B 2015, 119, 6081−6091

with thrombin (Nakalai Tesque, Kyoto, Japan) and was eluted. The eluted protein for sample 1 was further purified by DEAE ion exchange chromatography (GE healthcare, Buckinghamshire, UK). The labeling of sample 1 was performed as described previously.[29] The labeling of sample 2 is explained in the Supporting Information.

The bulk fluorescence spectra were obtained by using a fluorescence spectrometer (F-2500, Hitachi High Technologies, Tokyo, Japan) at room temperature (21−23 °C). The fluorescence intensities at different wavelength were calibrated by comparing a fluorescence spectrum of *N*,*N*-dimethyl-3-nitroanilin in 30% benzene and 70% hexane obtained by the spectrometer to a literature spectrum.[49] To obtain FRET efficiencies at the bulk condition, the fluorescence intensities after the intensity calibration was integrated from 500 to 625 nm and from 625 to 690 nm for the donor and acceptor dyes, respectively. Since the integrated regions were narrower than the entire fluorescence spectra, we then estimated the area ratios of the integrated regions to the entire fluorescence spectra provided by the manufacturers of the dyes. The area ratios were 0.95, 0.71, and 0.62 for Alexa488, Alexa633, and ATTO633, respectively. In addition, the contributions of leaks of the donor fluorescence to the acceptor spectrum were subtracted. The fluorescence quantum yields of 0.92 and 0.64 for Alexa488 and ATTO633, respectively, are provided by the manufacturers. While the yield for Alexa633 is not reported, we used a quantum yield of 0.23, which was estimated by comparing the integrated fluorescence intensity for Alexa633 to that of ATTO633 obtained in the same condition used as the standard.

Optical System for the Single-Molecule Measurements. The optical setup for the single-molecule fluorescence measurements was the same as reported previously.[29] In brief, the excitation light at 473 nm was obtained from a solid-state laser (SDL-473-LN-150T, Shanghai Dream Lasers Technology, Shanghai, China). The output was introduced to an objective (NA = 0.75, CFI S Fluor 20×, Nikon, Tokyo, Japan) after passing through a cylindrical lens (f = 70 mm). At the observation point, the beam formed an elliptic spot whose lengths of major and minor axes were ca. 0.4 mm and 1 μm, respectively. The excitation irradiance was on average 75−150 kW/cm^2 and did not exceed 500 kW/cm^2. The fluorescence was collected by the same objective, passed through the first dichroic mirror (Di01-R488-25×36, Semrock, Rochester, NY) and was spatially filtered by a slit set in parallel with the direction of the excitation spot. The donor and acceptor fluorescence were separated by using the second and third dichroic mirrors (NT49-471, Edmund, Barrington, NJ) and bandpass filters (FF01-536/40-25 and FF01-655/40-25, Semrock). The fluorescence images from the donor and acceptor dyes were detected simultaneously by using electron-bombarded CCD combined with image amplifier (C9400-01S, Hamamatsu Photonics, Hamamatsu, Japan).

Sample Delivery System for the Single-Molecule Measurements. The sample solution was introduced to a quartz microfluidic chip as reported previously.[29] The width, depth, and length of the observation channel were 5 μm, 20 μm, and 2 mm, respectively. A chromatography pump (DiNa-SS, KYA Technologies, Tokyo, Japan) was used to introduce the sample solution at the flow rate of 300 nL/min. The average line speed of the flowing molecules was 73 μm/ms (SD = 18). The residence time of a molecule at one pixel was 59 μs/pixel. Because of the blurring of a point light source (less than 2 pixels), the time resolution of the fluorescence time series was 120 μs.

Single-Molecule Fluorescence Measurements and the Data Analysis. The single-molecule fluorescence measurements were performed as reported previously.[29] The samples for the single-molecule measurements were prepared by dissolving the doubly labeled proteins into the buffer containing 20 mM Tris-HCl (pH 7.4) and various concentrations of guanidinium chloride (GdmCl). The buffer solution was filtered by filter with 0.22 μm pores (Millex-GS, Merck Millipore, Billerica, MA). Typically, 80 μL of the sample solution at concentrations between 0.1 and 1 nM was used for the detection of several hundreds of single-molecule traces in the observation time of several hours. All measurements were conducted at room temperature (21−23 °C). The basic procedures for the data analysis were the same as those reported previously;[29] however, details of the procedures were improved significantly. In particular, we improved the method to select the single-molecule traces by referencing to the background noise of each image. In addition, we estimated the FRET efficiencies by referencing to the fluorescence quantum yields, and the efficiencies of collecting photons by the current optical system. Furthermore, the RF values were reevaluated by considering the noise contributions from the background photons. The methods for the data analysis are described in Supporting Information.

RESULTS

Ensemble Fluorescence Measurements of the Labeled Mutants of BdpA. In our previous investigation, we prepared a triple mutant, Y15F/N22C/A55C, of BdpA.[29] The mutations were selected based on the fluorescence lifetime investigation, which used Y15F/N22C/A55W.[40] To the introduced cysteines, we labeled Alexa488 and Alexa633 (sample 1). The two sites are located at turn 1 and the C-terminus, whose Cα carbons in the native state of the wild-type protein are separated for 9 Å[31] (Figure 1). The proximity of the sites might lead to nearly 100% of the energy transfer for Alexa488 and Alexa633 having a Förster distance of 53.3 Å. The distance of the two sites in the unfolded state can be estimated as ca. 52 Å,[50] corresponding to the FRET efficiency of 0.54. The fluorescence spectra of sample 1 at different GdmCl concentrations are presented in Supporting Information Figure S1A. The data were the same as those described in our previous report;[29] however, the efficiency of detecting photons of the spectrometer was calibrated. The calibrated and integrated intensities of the donor (F_d) and acceptor (F_a) fluorescence and the bulk FRET efficiency (E) are plotted in Figure 2A. The FRET efficiency was calculated using eqs 1 and 2:

$$E = \frac{F_a}{F_a + \gamma F_d} \tag{1}$$

$$\gamma = \frac{\Phi_a \eta_a}{\Phi_d \eta_d} \tag{2}$$

where γ is the ratio of fluorescence quantum yield (Φ_a and Φ_d) and the efficiency of fluorescence detection (η_a and η_d) for the donor and acceptor and are described above. The FRET efficiencies thus estimated in the bulk condition were 0.98 and 0.80 for the native state at 0 M GdmCl and the unfolded state at 7 M GdmCl, respectively. Considering the uncertainty of the fluorescence quantum yields and the detection efficiencies of

DOI: 10.1021/acs.jpcb.5b00414
J. Phys. Chem. B 2015, 119, 6081−6091

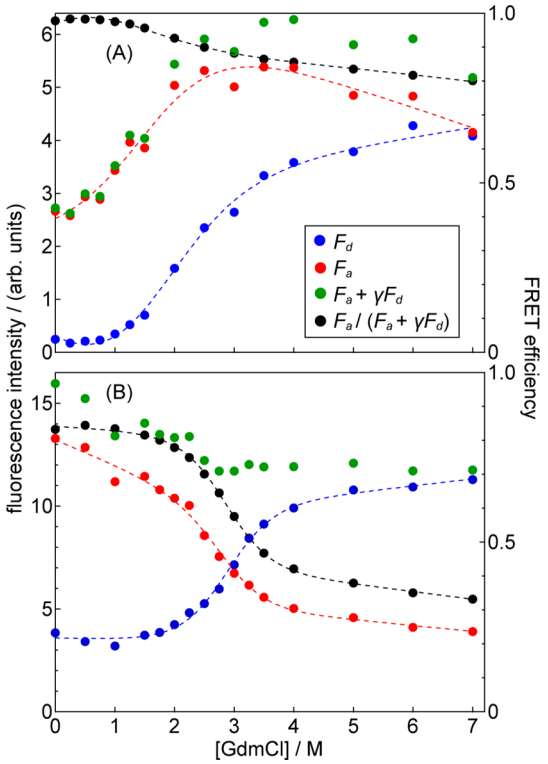

Figure 2. Equilibrium unfolding transitions of the labeled mutants of BdpA monitored by bulk fluorescence measurements. Panels A and B correspond to the data obtained for samples 1 and 2, respectively. The blue, red, and green symbols correspond to the integrated fluorescence intensities from the donor (F_d), acceptor (F_a), and their sum ($F_a + \gamma F_d$), respectively. The black symbols correspond to the FRET efficiency. The blue and red lines are the result of the global fitting of the donor and acceptor data, respectively, to the two-state mechanism with the same parameters. The black lines are the calculated FRET efficiencies based on the fitting results of the donor and acceptor intensities.

the apparatus, and the presence of linkers connecting the fluorophores and the protein, we interpret that the observed values are comparable to the expected efficiencies.

The intensities of the donor and acceptor fluorescence at different GdmCl concentrations behave anomalously (Figure 2A). The changes in the FRET efficiency might suggest that the donor and acceptor intensities reverse upon the unfolding transition; however, the donor and acceptor intensities both increase at the higher concentration of GdmCl. This can be explained by the quenching of the donor and acceptor fluorescence in the native state. Because of the proximity of the two fluorophores in the native state, a significant fraction of the fluorescence intensity might be diminished by the collisional quenching mechanism.[49] If we assume that the fluorescence intensity at 7 M GdmCl is free from the quenching effect, the plot of the sum of the donor and acceptor intensities ($F_a + \gamma F_d$) suggests that ca. 50% of the fluorescence intensity is quenched in the native state (Figure 2A).

The bulk unfolding curves of sample 1 can be explained based on the two-state transition. We fitted both the donor and acceptor fluorescence intensities globally by the two-state transition with the same parameters and obtained the m value and the unfolding free energy extrapolated to zero GdmCl concentration, ΔG_0 (Table 1). The fitting procedure is

Table 1. Stability of the Doubly Labeled Mutants of BdpA

	m (kcal mol^{-1} M^{-1})	ΔG_0 (kcal mol^{-1})
sample 1	0.87 ± 0.21	1.3 ± 0.5
sample 2	1.5 ± 0.2	4.3 ± 0.6
wild type[a]	1.5 ± 0.1	4.3 ± 0.2

[a]Data at 37 °C and at pH 5.0 from ref 31.

explained in the Supporting Information. The changes in the fluorescence intensities should be the sum of the two effects, i.e., the changes in the FRET efficiency and the quenching. However, a single transition is sufficient to explain both the donor and acceptor intensities, suggesting that the quenching occurs to a fixed fraction of the native component. We note that the FRET efficiency after the unfolding transition still changes as the increase in the GdmCl concentration, suggesting the gradual shift in the conformations of the unfolded state. In addition, the peak of the donor fluorescence spectrum changes slightly in the GdmCl concentration range from 0 to 1 M, suggesting the local environments of the donor might be altered (Supporting Information Figure S1A). Thus, the single unfolding transition based on the two-state model can explain the bulk fluorescence results of sample 1.

To avoid the quenching effect that complicates the interpretation of the data for sample 1 and to compare the behavior of different regions of BdpA, we constructed new labeling sites. We chose the sites near the N- and C-termini and introduced cysteine at residues 5 and 55 (K5C/Y15F/A55C). The distance between the Cα carbons of the two residues in the wild-type protein is 30 Å.[31] Thus, the collisional quenching in the native state might be avoided. We labeled the mutant by four combinations of donor and acceptor fluorophores. Among them, the sample labeled by Alexa488 and ATTO633 showed the best separation of the FRET efficiencies for the native and unfolded states (sample 2). The changes in the integrated fluorescence intensities of sample 2 upon the GdmCl titration are presented in Figure 2B. The raw fluorescence spectra are presented in Supporting Information Figure S1B. Sample 2 showed the reversal of donor and acceptor fluorescence intensities upon the unfolding, implying that the intensity changes are mainly governed by the FRET efficiency change alone. In comparison with sample 1, the sum of the donor and acceptor fluorescence intensities ($F_a + \gamma F_d$) showed less dependence on the GdmCl concentration (Figure 2B). Thus, we interpret that the quenching of the fluorescence intensity is minimized in sample 2.

The FRET efficiencies for sample 2 measured at the bulk level were 0.83 and 0.33 for the native state at 0 M GdmCl and the unfolded state at 7 M GdmCl, respectively. Based on the distance between the donor and acceptor residues for the native state (30 Å), that for the unfolded state (65 Å), and the Förster distance between Alexa488 and ATTO633 (50.8 Å), the FRET efficiencies can be estimated as 0.96 and 0.19 for the native and unfolded states, respectively. The estimations are consistent with the observed values. The unfolding curves of sample 2 can be explained based on the two-state transition. We could again fit the donor and acceptor fluorescence intensities globally by the two-state transition and obtained the fitting parameters (Table 1).

In summary, the bulk fluorescence results of the doubly labeled mutants of BdpA, samples 1 and 2, can be explained based on the two-state mechanism. While sample 1 showed a

DOI: 10.1021/acs.jpcb.5b00414
J. Phys. Chem. B 2015, 119, 6081−6091

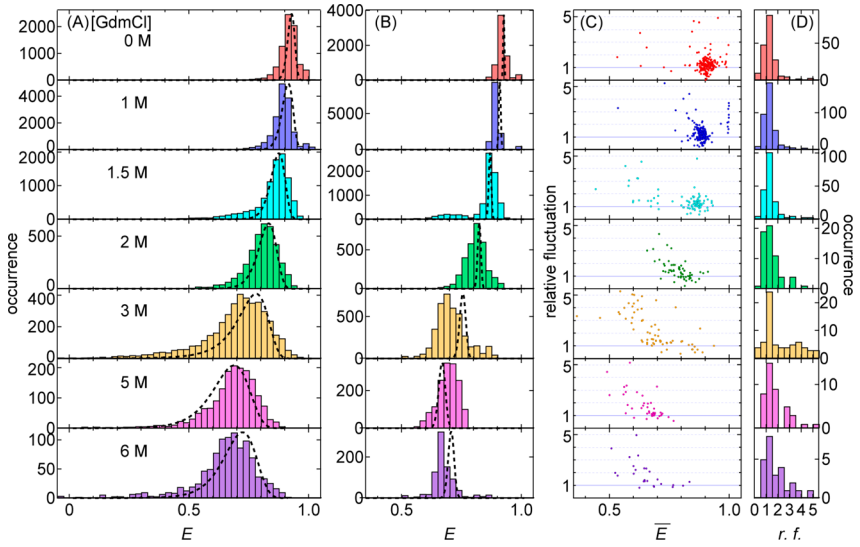

Figure 3. Equilibrium unfolding transition of sample 1 detected by single-molecule FRET measurements. Panel A presents the FRET distribution plots at different concentrations of GdmCl for the raw time series with the time resolution of 120 μs. Panel B presents the distribution plots after the moving time average of 1 ms. The dotted lines in panels A and B represent the theoretical distributions caused by photon shot noise estimated based on the averages of fluorescence intensity, FRET efficiency, and background photons for each data. Panel C presents the correlation plots between the average FRET efficiency and the RF values estimated for each trace with the time resolution of 120 μs. Panel D shows the histogram of the RF values.

significant quenching of its fluorescence in the native state, the quenching effect of sample 2 was reduced.

Measurements and Interpretation of sm-FRET Time Series for Sample 1. For the doubly labeled mutants of BdpA, we conducted sm-FRET time series measurements using the line confocal setup and the fast sample flow. We obtained the fluorescence intensity time series for the donor and acceptor, whose length is several milliseconds and time resolution is 120 μs. The temporal fluctuation of the raw data due to the spatial nonuniformity of the excitation light and to the diffusive motion of the sample molecules was eliminated by calculating the FRET efficiency using eq 1. In our early trials of the measurements, we utilized a buffer containing 10 mM phosphate and 100 mM NaCl at pH 7.4 in the presence of GdmCl but experienced irreversible changes in the sm-FRET data. That is, while the data look normal at the beginning of the measurements, the data having the FRET efficiency at around 0.7 began to appear at several tens of minutes after the sample injection. While the efficiency suggests the unfolded conformation, the signal could be detected even at the low denaturant concentrations. Several lines of evidence suggested that the traces appearing after several tens of minutes were originating from the samples once adsorbed on the surface of quartz microfluidic cell before the observation channel, desorbed from the surfaces, and reached to the observation region. To avoid the changes in the sm-FRET data, we searched for the condition in which the adsorption can be eliminated and found that by reducing the salt concentration the change of the FRET efficiency could be eliminated. We suggest that a charge repulsion between the negatively charged quartz surface and BdpA having pI around 5 can suppress the adsorption at low ionic strength. We conducted all the experiments in the solution containing 20 mM Tris-HCl at pH 7.4 and no salts and always confirmed that the sm-FRET data did not depend on the observation time. Furthermore, we completed all the measurements within several hours after the sample injection.

To examine the unfolding transition of sample 1, we obtained sm-FRET time traces at different concentrations of GdmCl. The FRET efficiency distributions for sample 1 are plotted in Figure 3A, which are based on the same data reported previously, but newly analyzed by using the improved data analysis procedures.[29] First, to extract traces with sufficiently low levels of noise, we modified the data selection procedure. Second, to examine the FRET efficiency defined by eq 1, not the fluorescence intensity ratio $(F_a/(F_a + F_d))$, we calibrated the fluorescence intensity by using fluorescence quantum yields of fluorophores and the detection efficiencies for donor and acceptor fluorophores. Third, we estimated theoretical noise distributions at the average photon counts, the average FRET efficiency, and the average background counts for each measurement. The theoretical noise distributions thus calculated are shown as dotted lines in Figure 3A. The detailed data analysis procedures are described in the Supporting Information.

We can assign the native and unfolded states in the FRET distribution plots for sample 1 (Figure 3A). From the bulk unfolding transition, sample 1 should be in the native state at 0 and 1 M GdmCl. Thus, the peak appearing at 0.9 and 0.88 at 0 and 1 M GdmCl, respectively, can be assigned to the native state (N). The data at 5 and 6 M GdmCl possess distributions at around 0.7 and can be assigned to the unfolded state (U). However, the assignment of the distributions near the folding midpoint requires further examination of the data.

To interpret the observed distributions for sample 1, we next compared the FRET distributions after the time averaging. The distributions in Figure 3A are for the raw data obtained at 120 μs time resolution. The distribution shapes observed are almost comparable to the theoretical distributions estimated based on the averages of FRET efficiencies, signal photon counts, and background photon counts, implying that the distributions for the raw data were mainly determined by the photon shot noise and the amplification noise of the CCD camera. However, the time averaging can increase the signal-to-noise ratio of the data

DOI: 10.1021/acs.jpcb.5b00414
J. Phys. Chem. B 2015, 119, 6081−6091

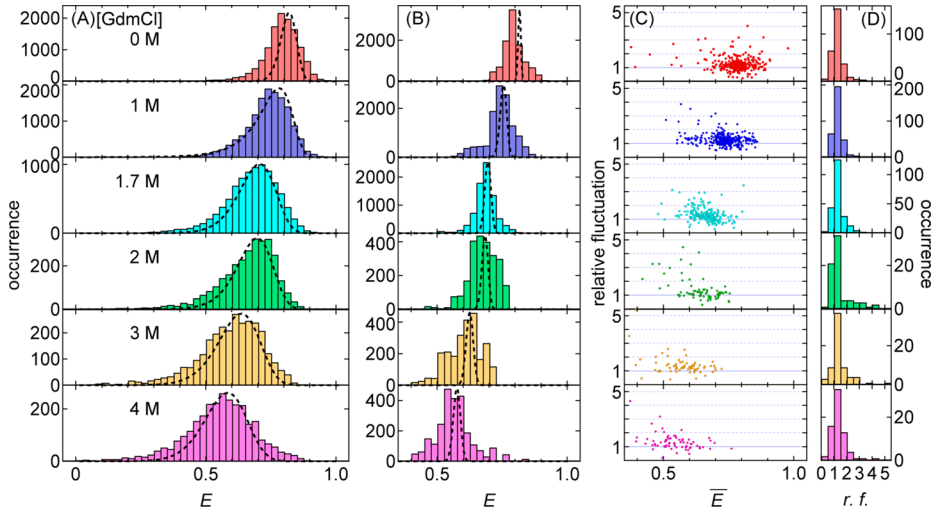

Figure 4. Equilibrium unfolding transition of sample 2 detected by single-molecule FRET measurements. Panel A presents the FRET distribution plots at different concentrations of GdmCl for the raw time series with the time resolution of 120 μs. Panel B presents the distribution plots after the moving time average of 1 ms. The dotted lines in panels A and B represent the theoretical distributions caused by photon shot noise estimated based on the averages of fluorescence intensity, FRET efficiency, and background photons for each data. Panel C presents the correlation plots between the average FRET efficiency and the RF values estimated for each trace with the time resolution of 120 μs. Panel D shows the histogram of the RF values.

and results in the narrowing of the FRET efficiency distribution. In addition, the time averaging might mix the exchanging states if the time constant of the averaging becomes longer than the time constant of the exchange. Thus, by comparing the distributions obtained after the time averaging, we may further obtain dynamical information on the data.

To increase the signal-to-noise ratio without decreasing the number of the data points, we carried out the moving averages of the time series of the donor and acceptor fluorescence intensities in the time axis for 1 ms and obtained the FRET efficiency histograms plotted in Figure 3B. The theoretical noise width for the time-averaged data was also presented as dotted lines. The distributions for N became impressively sharp after the time averaging and shift from 0.90 at 0 M GdmCl to 0.85 at 1.5 M GdmCl. The distribution at 2 M GdmCl is still broad even after the time averaging. As we will explain below, we interpret the data at 2 M GdmCl are the average of N and U. At 3 M GdmCl, the distribution after the time averaging possesses a main peak at 0.68 and minor peaks at around 0.8. Considering that sample 1 is mostly unfolded at 3 M GdmCl, we assign the peak at 0.68 to U. The distributions after the time averaging at 5 and 6 M GdmCl are still broad compared to the theoretical distributions. In addition, the minor peaks at around 0.8 detected at 3 M GdmCl disappeared. The results demonstrate that the unfolded state at the higher concentrations of GdmCl becomes expanded but retains a conformational heterogeneity.

To examine the dynamic properties of the time series, we compared the RF values for sample 1.[29] RF is calculated for each trace by dividing the standard deviation of the FRET efficiency trace (s) by the estimated shot noise width (σ) as defined in eq 3:

$$\mathrm{RF} = \frac{s}{\sigma} \tag{3}$$

where s is defined as eq 4:

$$s = \sqrt{\frac{1}{L-1}\sum_{i=1}^{L}(E(t_i)^2 - \bar{E}^2)} \tag{4}$$

In eq 4, L is the number of the data points in one trace, $E(t_i)$ is the FRET efficiency at time point t_i, and $\bar{E}$ is the FRET efficiency averaged over one trace as described in eq 5:

$$\bar{E} = \frac{1}{L}\sum_{i=1}^{L}E(t_i) \tag{5}$$

If a time series $E(t_i)$ has no time-dependent changes except for the shot noise, the RF value of the trace should be one. If a time series fluctuates due to the changes in the FRET efficiency, RF should be larger than one. In our previous investigation, the RF values were estimated based on the fluorescence intensity ratio ($F_a/(F_a + F_d)$) and without considering the noise contribution from the background photons (σ_b).[29] As discussed in the Supporting Information, we newly developed a method to calculate the RF values based on the FRET efficiency and to cancel the contribution of the background noise.

The two-dimensional plots in Figure 3C were the correlation between the average FRET efficiency and the RF value estimated for each trace with the time resolution of 120 μs. The histograms in Figure 3D are the plots of the RF values. The traces assigned to N at 0 and 1 M GdmCl possess the RF values mostly around 1. Thus, the traces in N showed small temporal fluctuations. In contrast, the RF values for many traces observed at 2 and 3 M GdmCl are appreciably larger than 1. A fraction of traces assigned to U at 5 and 6 M GdmCl also possess the RF values larger than 1. The data suggest that the traces fluctuate in the time scale longer than the time resolution of the current measurements (120 μs) but shorter than the observation duration (several milliseconds).

We interpret that the data for sample 1 at 2 M GdmCl indicate the exchange of N and U. In the GdmCl concentration range near the midpoint of the denaturation (~1.5 M), we expect to detect both U and N. However, the distributions for the raw data and for the 1 ms averaged data possess single

DOI: 10.1021/acs.jpcb.5b00414
J. Phys. Chem. B 2015, 119, 6081−6091

broad peak, suggesting the mixing of U and N. The higher RF values are also consistent with the mixing. If we assume that the folding rate constant of sample 1 is comparable to that of WT, the rate constant at 2 M GdmCl is $\sim 10^3$ s^{-1}, implying that the lifetime of U and N is shorter than the several milliseconds of observation time.[33] Accordingly, it is reasonable to assume that the mixing of U and N causes the single broad peak to appear in the FRET distribution plot. We further interpret that a fraction of traces observed at the GdmCl concentrations higher than 3 M showing the large RF values reflects the fluctuations of the traces within the unfolded state ensemble.

Measurements and Interpretation of sm-FRET Time Series for Sample 2. We next obtained the sm-FRET time series for sample 2 at several GdmCl concentrations and presented the FRET distribution plots in Figure 4A. The FRET distribution histograms obtained for the time-averaged traces for 1 ms are presented in Figure 4B. On the basis of the peaks in the time-averaged distributions, we can interpret that the peak appearing at the efficiency around 0.78 in the data at 0 M GdmCl to N. The peak for N shifts to lower efficiencies to 0.73 at 1 M and 0.65 at 2 M. In contrast, at 4 M GdmCl, the peak is centered at 0.53 and corresponds to U. At 3 M GdmCl, sample 2 is in the midpoint of folding transition, and the peaks should be assigned to N and U.

For the data at 2 M GdmCl, the peak detected at 0.65 is broad even after the time averaging of 1 ms and possess a shoulder at 0.73. Since sample 2 is in the native state based on the ensemble unfolding experiments, we interpret that the native state at 2 M GdmCl possesses a conformational heterogeneity. The heterogeneity is also observed in the data at 3 M GdmCl, where the distribution should be the mixture of N and U. In the time-averaged data, the distribution possesses three peaks at 0.69, 0.62, and 0.53. Among them, the peaks at 0.69 and 0.62 are likely assigned to N and that at 0.53 to U based on the comparison of the data at different GdmCl concentrations.

The RF values for the data obtained for sample 2 reveal the less dynamic behaviors of the traces compared to sample 1 (Figure 4C,D). The RF values for sample 2 at different concentrations of GdmCl are all centered around 1, demonstrating that the traces do not fluctuate significantly in the time scale longer than the time resolution of the current measurements (120 μs). In contrast to the result for sample 1, sample 2 near the unfolding midpoint (3 M GdmCl) showed distinct peaks assignable to N and U. The RF values for the peaks are centered around 1, suggesting that the mixing of N and U does not occur for sample 2. This is reasonable observation since the folding rate constant at 3 M GdmCl is expected to become 100−200 s^{-1}, meaning that both U and N states should possess lifetime longer than the observation time of the current apparatus.[33] Accordingly, the current results are consistent with the reported dynamic properties of BdpA.

DISCUSSION

Complexity of the Folding Transition of the Labeled BdpA Identified in the Bulk and Single-Molecule Measurements. We will first discuss the folding mechanism of the doubly labeled BdpA revealed through the bulk and single-molecule fluorescence measurements. The bulk fluorescence spectra for the unfolding transition of sample 1 showed the significant fluorescence quenching in the native state in addition to the changes in the FRET efficiency. However, a single unfolding transition is sufficient to explain the changes in both of the donor and acceptor fluorescence intensities, suggesting that the quenching occurs to a fixed fraction of the native state for sample 1. Since the sum of the donor and acceptor fluorescence intensity ($F_a + \gamma F_d$) at 0 M GdmCl is ca. 50% of that at 7 M GdmCl, we interpret that ca. 50% of the native state population possesses the quenched fluorescence intensity likely caused by the collisional quenching of the donor and acceptor that are located in the proximity in the native state.

The fraction emitting the fluorescence at the low denaturant concentrations should not be in the unfolded state but in the native state. First, the FRET efficiency of the component in the zero denaturant concentration is 0.90, showing a short donor−acceptor distance. Second, the average FRET efficiency at the bulk level shows a sigmoidal change upon the increase in the GdmCl concentration, which is usually ascribed to the unfolding transition. If the emitting component is originating from the unfolded state, the FRET efficiency should change less cooperatively. Third, the population of the emitting component at the zero denaturant is ca. 50%, which is too large to be accounted for by the unfolded component in the native condition. Thus, we interpret that the native population of sample 1 has two components: the quenched native component (N_q) and the emitting native component (N_e).

The two components of the native state might be either the distinct states separated by an energy barrier or the states that mix rapidly. We suggest that the latter possibility is more likely, since population of N_q and N_e changes in parallel each other. If N_q and N_e are the distinct states, one of which possesses the partially disordered structures, the relative population of N_q and N_e should change as the function of denaturant, causing two transitions in the bulk unfolding curve. However, the current titration results can be explained by a single transition. In addition, if N_e and N_q exchange in the time domain accessible to the current measurement system, single-molecule fluorescence intensities of sample 1 at the low denaturant concentrations should exhibit intermittent behavior. However, we did not detect signals showing the intermittent behavior among 2074 molecules of sample 1 in the GdmCl concentration range from 0 to 1.5 M. We suggest that N_q and N_e are distinct in the time domain of fluorescence lifetime (several nanoseconds) but are mixed in the time domain of our observation (120 μs). We propose that the difference between N_q and N_e is the local conformational change around the fluorophores that are not affected by the GdmCl concentration.

In addition to N_q and N_e observed for sample 1, the current results revealed complexities in the folding transition of the labeled BdpA. First, the distribution peak for N shifts as the function of GdmCl for both samples 1 and 2, implying that the conformation of the native state swells at the increased denaturant concentrations. Second, the FRET distribution peaks for U are broad for both samples 1 and 2, demonstrating the significant conformational heterogeneity in the unfolded state. Third, a broadening of the distribution for N at the moderate concentration of GdmCl was observed for sample 2. These results demonstrate that the flexibility and the heterogeneity of the native and unfolded state structures for BdpA.

BdpA is considered as one of the representative examples of the two-state proteins. Except for the intermediate caused by the cis−trans isomerization of proline residues,[33,39] the accumulated data on BdpA all indicated the two-state folding. These include the linear chevron plots, absence of a burst phase

DOI: 10.1021/acs.jpcb.5b00414
J. Phys. Chem. B 2015, 119, 6081−6091

in the kinetic folding and unfolding experiments, and single sigmoidal curve for the static unfolding transition.[32−35] However, the evidence does not rule out the changes in the native state conformation and the broad distributions in the unfolded state. As long as the substates exchange faster than the folding or unfolding times, the apparent two-state behavior can be maintained. Similar features are detected for other proteins. In the case for SH3, another example of the two-state proteins, the swelling of the native state structure was suggested based on the fluorescence lifetime measurements.[12] Im9 also demonstrated the shift of the FRET efficiency assigned to the native state.[51] The detected complexity of the unfolding transition of BdpA is consistent with the accumulated evidence supporting the two-state folding.

Conformational and Dynamical Properties of N. We will next discuss the structural and dynamical properties of N. In sample 1, the residues at turn 1 (Asn22) and the C-terminus (Ala55) were substituted for cysteine and labeled. In the native state of the wild-type protein, Asn22 is located in the well-structured region, whose side chain is half buried by Pro21, Asn53, and Ala57.[31] The site at the C-terminus, Ala55, is surface exposed and is in the border between the structured and fluctuating regions.[31] Thus, the labeling at the residue 22 for sample 1 partially disrupts the structure of N, causing the reduction of ΔG_0 and m (Table 1). In sample 2, the labeling was introduced near the N- and C-termini (5 and 55). The labeling site at the N-terminus, residue 5, is located in the fluctuating region. The stability parameters of sample 2 are comparable to those of the wild-type protein (Table 1) and demonstrate the small structural effect of the labeling.

In the preunfolding region of the GdmCl concentrations, we detected the shift of the native state structure for both samples 1 and 2, suggesting the swelling of the distance between the labeling sites. A possibility that the shift might be caused by the kinetic mixing and averaging of the unfolded state is unlikely, since the shift is similarly observed for both samples 1 and 2 irrespective of the stability difference. In addition to the shift in the native state efficiency, the native state distribution becomes broader near the unfolding midpoint of sample 2. We propose that the region in the N-terminal part of BdpA likely contributes to the structural heterogeneity of the native state. In the NMR investigation of BdpA, residues from 1 to 9 were highly fluctuating.[31] In addition, the amide protons up to residues 15 exchange faster than the core domain.[32] Similarly, the C-terminal residues after residue 52 are flanking and might explain the swelling of N at the elevated concentration of GdmCl.[31,32]

It is tempting to compare the current results to those of the molecular dynamics calculation for BdpA reported by Maisuradze et al.[47] They calculated the temperature unfolding transition of BdpA and showed that the conformation of BdpA gradually shifts from the native structure to the unfolded structure at the higher temperature and concluded that the folding of BdpA might obey the downhill folding at the higher temperature. While the current and previous data obtained for BdpA at the room temperature are consistent with the two-state mechanism, the gradual expansion of the native state structure of BdpA at the higher concentration of GdmCl might be consistent with the calculation results. Further examination of the folding transition of BdpA at the higher temperature is warranted.

Conformational and Dynamical Properties of U. We will next discuss the structures of U in the post-unfolding region. In sample 1 at 3 M GdmCl, we identified the broad distribution of U. The peak FRET efficiency of U (0.68) can be explained by assuming a random coil chain having the donor and acceptor distance of 49 Å. The minor peaks of U at around 0.80 can be converted into the distance of 44 Å. The observation might be consistent with the fluorescence lifetime measurements, in which the distance between the same residues labeled in sample 1 was estimated to be 22−24 Å at the GdmCl concentration of 1.7−2.4 M.[40] At the higher concentration of GdmCl (4.0−5.0 M), the lifetime measurements suggested the donor−acceptor distance of 30−40 Å. While the current results gave longer estimates, the compact and expanded conformations for U near the unfolding midpoint and at the higher concentration of GdmCl, respectively, were reproduced.

A prominent property of the traces observed for the unfolded state is the heterogeneity. While the FRET efficiency distributions for the raw data are comparable to the theoretical shot noise width, the distributions after the time averaging for the unfolded state are significantly broader than the theoretical width (Figures 3 and 4). The broadening is caused by the slightly different FRET efficiencies detected for different protein molecules. We presented examples of the unfolded traces for samples 1 and 2 in Figure 5, which are selected from the traces having higher photon count rate and possess much narrower shot noise width compared to the average. While the

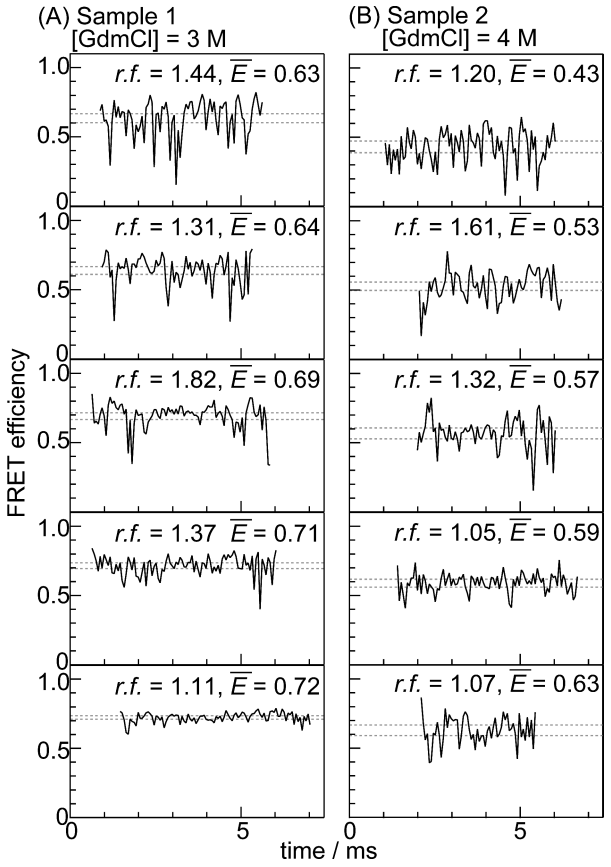

Figure 5. Examples of the traces observed for the unfolded state of sample 1 (panel A) and sample 2 (panel B). The selected traces observed in the presence of GdmCl at 3 M for sample 1 and at 4 M for sample 2 were presented. The dashed lines represent the noise width calculated based on the numbers of fluorescence and background photons for each trace.

DOI: 10.1021/acs.jpcb.5b00414
J. Phys. Chem. B 2015, 119, 6081−6091

individual traces fluctuate at around certain efficiency without significant time-dependent changes, the different traces possess different efficiencies. In both samples 1 and 2, many traces show nearly constant FRET efficiency. However, a small fraction of traces observed for U showed fluctuations that might be assigned to the jumps among different FRET efficiencies. The number of such traces was small, suggesting that the transitions among different FRET values mostly occur in the time domain longer than a few milliseconds.

The heterogeneity of the sm-FRET data has been frequently observed for other systems as the distribution width broader than the shot noise width. In the case for the double-stranded DNA with donor and acceptor fluorophores at the both termini, the broad distributions were sometimes observed.[52−54] Based on the comparison of the numbers of the donor and acceptor photons and from the lifetime of the donor fluorescence, it was inferred that the apparent heterogeneity might be caused by the difference in the quantum efficiency of the acceptor fluorescence caused by the local structural variation.[54] In the case for proteins, the unfolded ensembles frequently possess the broader distribution compared to that of the shot noise width. The broadening might be ascribed to the sample heterogeneity caused by the immobilization.[55] However, the unfolded state of many proteins observed in freely diffusing mode showed the broader distributions.[22−24,51]

A further difficulty in the interpretation of the apparent heterogeneity is the fastness of the conformational fluctuations deduced for the unfolded proteins.[17] The unfolded proteins are fluctuating at a very fast time scale. Based on the single-molecule correlation method, a time constant of several tens of nanoseconds was reported as the time scale for the donor−acceptor distance fluctuation.[56] Given the fastness of the fluctuating motion, the presence of structural heterogeneity that last more than several milliseconds is paradoxical. Thus, the broad distribution for the unfolded ensemble might be a general phenomenon; however, it is difficult to explain the observations consistently.

To explain the apparent heterogeneity of the observed traces, we propose the hierarchal chain dynamics in the unfolded state of the labeled BdpA. We assume that there remain residual structures in several localized parts of the unfolded chain including the parts near the labeling sites. The structures should be slightly different from molecule to molecule, and the transitions among different local structures can take more than a few milliseconds. Thus, the local environment of the fluorophores can be heterogeneous, causing different FRET efficiencies or different fluorescence quantum yields for different protein molecules in the unfolded state. There should exist the fast relaxation dynamics in the unfolded BdpA, which should involve the changes in the FRET efficiency within the time resolution (120 μs). However, the residual local structures around the fluorophores can cause the heterogeneity of the observed traces. Further examination is required to understand the apparent heterogeneity of the unfolded ensemble of BdpA.

In summary, the current data based on the line confocal microscopy resolved the complexity of the folding transition of BdpA usually hidden in the apparent two state folding. We detected the swelling and flexibility of the native state structure and the heterogeneity of the unfolded state. In addition, the motional mixing of the FRET peaks was suggested. The RF values can be used to deduce the dynamical properties of the molecules in the observation time period. The fast time-resolved measurements and the high resolution detection of FRET efficiencies enabled by the line-confocal microscopy will further clarify the heterogeneity and dynamics of biological molecules.

■ ASSOCIATED CONTENT

Supporting Information

Figures for the equilibrium unfolding transition of the doubly labeled BdpA; method information for the sample labeling, the fitting procedure for the unfolding transition, the data extraction of the single-molecule time traces, and the theoretical noise distribution of the FRET efficiency and the calculation of relative fluctuation. The Supporting Information is available free of charge on the ACS Publications website at DOI: 10.1021/acs.jpcb.5b00414.

■ AUTHOR INFORMATION

Corresponding Author

*E-mail: st@tagen.tohoku.ac.jp (S.T.).

Author Contributions

H.O., K.K., M.A., and S.T. designed the experiments. H.O. performed the experiments. M.A. expressed and purified BdpA. H.O. labeled BdpA. H.O., K.K., M.A., and S.T. wrote the paper and Supporting Information. All authors have given approval to the final version of the manuscript.

Notes

The authors declare no competing financial interest.

■ ACKNOWLEDGMENTS

This work was supported by Grants-in-Aid for Scientific Research from the Ministry of Education, Culture, Sports, Science and Technology of Japan to K.K, M.A., and S.T. M.A. was supported by the Asahi Glass Foundation and by Japan Science and Technology Agency, PRESTO. H.O., K.K., and S.T. thank Drs. Tahara, Ishii and Otosu at RIKEN for the discussion on the interpretation of the fluorescence data.

■ ABBREVIATIONS

SMFS, single-molecule fluorescence spectroscopy; FRET, fluorescence resonance energy transfer; BdpA, the B domain of protein A; RF, relative fluctuation; GdmCl, guanidinium chloride.

■ REFERENCES

(1) Baldwin, R. L.; Rose, G. D. Molten Globules, Entropy-Driven Conformational Change and Protein Folding. *Curr. Opin. Struct. Biol.* **2013**, *23*, 4−10.

(2) Udgaonkar, J. B. Polypeptide Chain Collapse and Protein Folding. *Arch. Biochem. Biophys.* **2013**, *531*, 24−33.

(3) Dill, K. A.; MacCallum, J. L. The Protein-Folding Problem, 50 Years On. *Science* **2012**, *338*, 1042−1046.

(4) Sosnick, T. R.; Barrick, D. The Folding of Single Domain Proteins - Have We Reached a Consensus? *Curr. Opin. Struct. Biol.* **2011**, *21*, 12−24.

(5) Kathuria, S. V.; Guo, L.; Graceffa, R.; Barrea, R.; Nobrega, R. P.; Matthews, C. R.; Irving, T. C.; Bilsel, O. Structural Insights into Early Folding Events Using Continuous-Flow Time-Resolved Small-Angle X-Ray Scattering. *Biopolymers* **2011**, *95*, 550−558.

(6) Buchner, G. S.; Murphy, R. D.; Buchete, N. V.; Kubelka, J. Dynamics of Protein Folding: Probing the Kinetic Network of Folding−Unfolding Transitions with Experiment and Theory. *Biochim. Biophys. Acta* **2011**, *1814*, 1001−1020.

(7) Takahashi, S.; Kamagata, K. Staring at a Protein: Ensemble and Single-Molecule Investigations on Protein-Folding Dynamics. In *Single Molecule Biophysics: Experiments and Theories*; Komatsuzaki, T.,

DOI: 10.1021/acs.jpcb.5b00414
J. Phys. Chem. B 2015, 119, 6081−6091

Takahashi, S., Kawakami, M., Yang, H., Silbey, R., Eds.; Advances in Chemical Physics 146; Wiley: Hoboken, NJ, 2011; pp 3−22.
(8) Jackson, S. E. How Do Small Single-Domain Proteins Fold? *Folding Des.* **1998**, *3*, R81−91.
(9) Barrick, D. What Have We Learned from the Studies of Two-State Folders, and What Are the Unanswered Questions about Two-State Protein Folding? *Phys. Biol.* **2009**, 015001.
(10) Bai, Y.; Zhou, H.; Zhou, Y. Critical Nucleation Size in the Folding of Small Apparently Two-State Proteins. *Protein Sci.* **2004**, *13*, 1173−1181.
(11) Naganathan, A. N.; Muñoz, V. Thermodynamics of Downhill Folding: Multi-Probe Analysis of PDD, a Protein That Folds Over a Marginal Free Energy Barrier. *J. Phys. Chem. B* **2014**, *118*, 8982−8994.
(12) Kishore, M.; Krishnamoorthy, G.; Udgaonkar, J. B. Critical Evaluation of the Two-State Model Describing the Equilibrium Unfolding of the PI3K SH3 Domain by Time-Resolved Fluorescence Resonance Energy Transfer. *Biochemistry* **2013**, *52*, 9482−9496.
(13) Spudich, G. M.; Miller, E. J.; Marqusee, S. Destabilization of The *Escherichia coli* RNase H Kinetic Intermediate: Switching Between a Two-State and Three-State Folding Mechanism. *J. Mol. Biol.* **2004**, *335*, 609−618.
(14) Moerner, W. E. New Directions in Single-Molecule Imaging and Analysis. *Proc. Natl. Acad. Sci. U.S.A.* **2007**, *104*, 12596−12602.
(15) Michalet, X.; Weiss, S.; Jäger, M. Single-Molecule Fluorescence Studies of Protein Folding and Conformational Dynamics. *Chem. Rev.* **2006**, *106*, 1785−1813.
(16) Roy, R.; Hohng, S.; Ha, T. A Practical Guide to Single-Molecule FRET. *Nat. Methods* **2008**, *5*, 507−516.
(17) Schuler, B.; Hofmann, H. Single-Molecule Spectroscopy of Protein Folding Dynamics–Expanding Scope and Timescales. *Curr. Opin. Struct. Biol.* **2013**, *23*, 36−47.
(18) Krivov, S. V.; Karplus, M. Hidden Complexity of Free Energy Surfaces for Peptide (Protein) Folding. *Proc. Natl. Acad. Sci. U.S.A.* **2004**, *101*, 14766−14770.
(19) Rao, F.; Caflisch, A. The Protein Folding Network. *J. Mol. Biol.* **2004**, *342*, 299−306.
(20) Rylance, G. J.; Johnston, R. L.; Matsunaga, Y.; Li, C. B.; Baba, A.; Komatsuzaki, T. Topographical Complexity of Multidimensional Energy Landscapes. *Proc. Natl. Acad. Sci. U.S.A.* **2006**, *103*, 18551−18555.
(21) Hori, N.; Chikenji, G.; Berry, R. S.; Takada, S. Folding Energy Landscape and Network Dynamics of Small Globular Proteins. *Proc. Natl. Acad. Sci. U.S.A.* **2009**, *106*, 73−78.
(22) Talaga, D. S.; Lau, W. L.; Roder, H.; Tang, J.; Jia, Y.; DeGrado, W. F.; Hochstrasser, R. M. Dynamics and Folding of Single Two-Stranded Coiled-Coil Peptides Studied by Fluorescent Energy Transfer Confocal Microscopy. *Proc. Natl. Acad. Sci. U.S.A.* **2000**, *97*, 13021−13026.
(23) Deniz, A. A.; Laurence, T. A.; Beligere, G. S.; Dahan, M.; Martin, A. B.; Chemla, D. S.; Dawson, P. E.; Schultz, P. G.; Weiss, S. Single-Molecule Protein Folding: Diffusion Fluorescence Resonance Energy Transfer Studies of the Denaturation of Chymotrypsin Inhibitor 2. *Proc. Natl. Acad. Sci. U.S.A.* **2000**, *97*, 5179−5184.
(24) Schuler, B.; Lipman, E. A.; Eaton, W. A. Probing the Free-Energy Surface for Protein Folding with Single-Molecule Fluorescence Spectroscopy. *Nature* **2002**, *419*, 743−747.
(25) Rhoades, E.; Gussakovsky, E.; Haran, G. Watching Proteins Fold One Molecule at a Time. *Proc. Natl. Acad. Sci. U.S.A.* **2003**, *100*, 3197−3202.
(26) Kinoshita, M.; Kamagata, K.; Maeda, A.; Goto, Y.; Komatsuzaki, T.; Takahashi, S. Development of a Technique for the Investigation of Folding Dynamics of Single Proteins for Extended Time Periods. *Proc. Natl. Acad. Sci. U.S.A.* **2007**, *104*, 10453−10458.
(27) Kamagata, K.; Kawaguchi, T.; Iwahashi, Y.; Baba, A.; Fujimoto, K.; Komatsuzaki, T.; Sambongi, Y.; Goto, Y.; Takahashi, S. Long-Term Observation of Fluorescence of Free Single Molecules to Explore Protein-Folding Energy Landscapes. *J. Am. Chem. Soc.* **2012**, *134*, 11525−11532.
(28) Campos, L. A.; Liu, J.; Wang, X.; Ramanathan, R.; English, D. A.; Muñoz, V. A Photoprotection Strategy for Microsecond-Resolution Single-Molecule Fluorescence Spectroscopy. *Nat. Methods* **2011**, *8*, 143−146.
(29) Oikawa, H.; Suzuki, Y.; Saito, M.; Kamagata, K.; Arai, M.; Takahashi, S. Microsecond Dynamics of an Unfolded Protein by a Line Confocal Tracking of Single Molecule Fluorescence. *Sci. Rep.* **2013**, *3*, 2151.
(30) Horrocks, M. H.; Li, H.; Shim, J. U.; Ranasinghe, R. T.; Clarke, R. W.; Huck, W. T.; Abell, C.; Klenerman, D. Single Molecule Fluorescence under Conditions of Fast Flow. *Anal. Chem.* **2012**, *84*, 179−185.
(31) Gouda, H.; Torigoe, H.; Saito, A.; Sato, M.; Arata, Y.; Shimada, I. Three-Dimensional Solution Structure of the B Domain of Staphylococcal Protein A: Comparisons of the Solution and Crystal Structures. *Biochemistry* **1992**, *31*, 9665−9672.
(32) Bai, Y.; Karimi, A.; Dyson, H. J.; Wright, P. E. Absence of a Stable Intermediate on the Folding Pathway of Protein A. *Protein Sci.* **1997**, *6*, 1449−1457.
(33) Myers, J. K.; Oas, T. G. Preorganized Secondary Structure as an Important Determinant of Fast Protein Folding. *Nat. Struct. Biol.* **2001**, *8*, 552−558.
(34) Arora, P.; Oas, T. G.; Myers, J. K. Fast and Faster: A Designed Variant of the B-domain of Protein A Folds in 3 μsec. *Protein Sci.* **2004**, *13*, 847−853.
(35) Sato, S.; Religa, T. L.; Daggett, V.; Fersht, A. R. Testing Protein-Folding Simulations by Experiment: B Domain of Protein A. *Proc. Natl. Acad. Sci. U.S.A.* **2004**, *101*, 6952−6956.
(36) Sato, S.; Religa, T. L.; Fersht, A. R. Φ-Analysis of the Folding of the B Domain of Protein A Using Multiple Optical Probes. *J. Mol. Biol.* **2006**, *360*, 850−864.
(37) Sato, S.; Fersht, A. R. Searching for Multiple Folding Pathways of a Nearly Symmetrical Protein: Temperature Dependent Φ-Value Analysis of the B Domain of Protein A. *J. Mol. Biol.* **2007**, *372*, 254−267.
(38) Huang, F.; Sato, S.; Sharpe, T. D.; Ying, L.; Fersht, A. R. Distinguishing Between Cooperative and Unimodal Downhill Protein Folding. *Proc. Natl. Acad. Sci. U.S.A.* **2007**, *104*, 123−127.
(39) Hoffmann, A.; Nettels, D.; Clark, J.; Borgia, A.; Radford, S. E.; Clarke, J.; Schuler, B. Quantifying Heterogeneity and Conformational Dynamics from Single Molecule FRET of Diffusing Molecules: Recurrence Analysis of Single Particles (RASP). *Phys. Chem. Chem. Phys.* **2011**, *13*, 1857−1871.
(40) Huang, F.; Lerner, E.; Sato, S.; Amir, D.; Haas, E.; Fersht, A. R. Time-Resolved Fluorescence Resonance Energy Transfer Study Shows a Compact Denatured State of the B Domain of Protein A. *Biochemistry* **2009**, *48*, 3468−3476.
(41) Boczko, E. M.; Brooks, C. L., III. First-Principles Calculation of the Folding Free Energy of a Three-Helix Bundle Protein. *Science* **1995**, *269*, 393−396.
(42) Zhou, Y.; Karplus, M. Interpreting the Folding Kinetics of Helical Proteins. *Nature* **1999**, *401*, 400−403.
(43) Alonso, D. O.; Daggett, V. Staphylococcal Protein A: Unfolding Pathways, Unfolded States, and Differences between the B and E Domains. *Proc. Natl. Acad. Sci. U.S.A.* **2000**, *97*, 133−138.
(44) García, A. E.; Onuchic, J. N. Folding a Protein in a Computer: An Atomic Description of the Folding/Unfolding of Protein A. *Proc. Natl. Acad. Sci. U.S.A.* **2003**, *100*, 13898−13903.
(45) Vila, J. A.; Ripoll, D. R.; Scheraga, H. A. Atomically Detailed Folding Simulation of the B Domain of Staphylococcal Protein A from Random Structures. *Proc. Natl. Acad. Sci. U.S.A.* **2003**, *100*, 14812−14816.
(46) Itoh, K.; Sasai, M. Flexibly Varying Folding Mechanism of a Nearly Symmetrical Protein: B Domain of Protein A. *Proc. Natl. Acad. Sci. U.S.A.* **2006**, *103*, 7298−7303.
(47) Maisuradze, G. G.; Liwo, A.; Ołdziej, S.; Scheraga, H. A. Evidence, from Simulations, of a Single State with Residual Native Structure at the Thermal Denaturation Midpoint of a Small Globular Protein. *J. Am. Chem. Soc.* **2010**, *132*, 9444−9452.

DOI: 10.1021/acs.jpcb.5b00414
J. Phys. Chem. B 2015, 119, 6081−6091

(48) Kachlishvilia, K.; Maisuradzea, G. G.; Martina, O. A.; Liwoc, A.; Vila, J. A.; Scheraga, H. A. Accounting for a Mirror-Image Conformation as a Subtle Effect in Protein Folding. *Proc. Natl. Acad. Sci. U.S.A.* **2014**, *111*, 8458−8463.
(49) Lakowicz, J. R. *Principles of Fluorescence Spectroscopy*, 2nd ed.; Kluwer Academic/Plenum Publishers: New York, 1999; p 641.
(50) Hoffmann, A.; Kane, A.; Nettels, D.; Hertzog, D. E.; Baumgärtel, P.; Lengefeld, J.; Reichardt, G.; Horsley, D. A.; Seckler, R.; Bakajin, O.; Schuler, B. Mapping Protein Collapse with Single-Molecule Fluorescence and Kinetic Synchrotron Radiation Circular Dichroism Spectroscopy. *Proc. Natl. Acad. Sci. U.S.A.* **2007**, *104*, 105−110.
(51) Tezuka-Kawakami, T.; Gell, C.; Brockwell, D. J.; Radford, S. E.; Smith, D. A. Urea-Induced Unfolding of the Immunity Protein Im9 Monitored by spFRET. *Biophys. J.* **2006**, *12*, L42−44.
(52) Nir, E.; Michalet, X.; Hamadani, K. M.; Laurence, T. A.; Neuhauser, D.; Kovchegov, Y.; Weiss, S. Shot-Noise Limited Single-Molecule FRET Histograms: Comparison between Theory and Experiments. *J. Phys. Chem. B* **2006**, *110*, 22103.
(53) Vogelsang, J.; Doose, S.; Sauer, M.; Tinnefeld, P. Single-Molecule Fluorescence Resonance Energy Transfer in Nanopipets: Improving Distance Resolution and Concentration Range. *Anal. Chem.* **2007**, *79*, 7367.
(54) Kalinin, S.; Sisamakis, E.; Magennis, S. W.; Felekyan, S.; Seidel, C. A. M. On the Origin of Broadening of Single-Molecule FRET Efficiency Distributions beyond Shot Noise Limits. *J. Phys. Chem. B* **2010**, *114*, 6197−6206.
(55) Chung, H. S.; Louis, J. M.; Eaton, W. A. Distinguishing between Protein Dynamics and Dye Photophysics in Single-Molecule FRET Experiments. *Biophys. J.* **2010**, *98*, 696−706.
(56) Nettels, D.; Gopich, I. V.; Hoffmann, A.; Schuler, B. Ultrafast Dynamics of Protein Collapse from Single-Molecule Photon Statistics. *Proc. Natl. Acad. Sci. U.S.A.* **2007**, *104*, 2655−2660.

DOI: 10.1021/acs.jpcb.5b00414
J. Phys. Chem. B 2015, 119, 6081−6091